J Therm Anal Calorim
DOI 10.1007/s10973-013-3250-9

Synthesis, thermal and infrared spectroscopic studies of hydrazinated mixed metal fumarates

U. B. Gawas · V. M. S. Verenkar

Received: 20 October 2012 / Accepted: 10 May 2013

Abstract A series of hydrazinated complexes of mixed nickel manganese zinc ferrous fumarates were synthesized from aqueous metal chlorides solution and sodium fumarate–hydrazine hydrate mixture. These complexes were characterized by chemical analysis, infrared spectroscopy, thermogravimetry-differential scanning calorimetry and isothermal mass loss studies. The hydrazine ligand in these complexes shows bidentate bridging nature while, carboxylate ion displays monodentate behaviour. Thermal decomposition studies indicate 3-step decomposition, involving 2-step dehydrazination and 1-step decarboxylation. The thermal decomposition residues were characterized by X-ray diffractometry, transmission electron microscopy and infrared spectroscopy.

Keywords Hydrazinated mixed metal fumarates · Thermal analysis · Nano-particle · Ferrites

Introduction

Metal carboxylates and dicarboxylates have been extensively investigated for their thermal behaviour as well as their use as precursors for ultrafine particle metal oxides of technological importance [1–3]. The synthesis and characterization of many such complexes have been reported with aliphatic carboxylates and dicarboxylates such as formate [2, 4], acetate [5], oxalate [6–8], malonate [9], succinate [3, 10], malate [11], citrate [12], tartrate [13], maleate and fumarate [14–16]. Among the dicarboxylates, the transition metal fumarate complexes usually exhibit versatile and interesting coordination modes and framework topologies; since the dicarboxylate group of fumaric acid can act as both monodentate and multidentate ligand [17–21]. More importantly, the thermal decomposition residue obtained after decomposition finds extensive applications. With the advent of nanotechnology the search for the new and better synthetic techniques has gained momentum due to the interesting magnetic and optical properties displayed by metal as well as metal oxide nanoparticles which are significantly different from their bulk counterpart. One such approach is the use of hydrazinated carboxylate and dicarboxylate complexes as precursors, since these complexes decompose at lower temperature providing easy access to obtain the nanoparticles. The synthesis and thermal studies on many hydrazinated metal carboxylates and dicarboxylates, such as formate [22], acetate [23, 24], oxalate [25–27], malonates and succinates [24, 28–30], malate [31], maleate and fumarate [32] have been reported. Our group has used hydrazinated metal/mixed metal fumarate complexes as precursors to prepare nanocrystalline ceramic oxides like $NiMn_2O_4$ [33], $NiFe_2O_4$ [34], Ni–Zn ferrites [35], Mn–Zn ferrites [36], Co–Zn ferrites [37–40] and Co–Ni ferrites [41, 42]. Recently, we have used this method to prepare multi-substituted ferrites viz. Ni–Mn–Zn-ferrites [43–45]. In continuation of this study, the preparation of $Mn_xNi_{0.6-x}Zn_{0.4}Fe_2O_4$ ($x = 0.2$, 0.4 and 0.5) ferrites from their hydrazinated mixed nickel manganese zinc ferrous fumarate complexes, $Mn_xNi_{0.6-x}Zn_{0.4}Fe_2(C_4H_2O_4)_3{\cdot}6N_2H_4$ ($x = 0.2$, 0.4 and 0.5) has been undertaken.

Experimental

All reagents used were of analytical grade supplied by s.d. Fine-Chem Ltd., India except iron powder. The

U. B. Gawas · V. M. S. Verenkar (✉)
Department of Chemistry, Goa University, Taleigao Plateau, Goa 403206, India
e-mail: vmsv@rediffmail.com

Published online: 11 June 2013

stoichiometric quantities of metal chloride of manganese, zinc and nickel were dissolved in distilled water to achieve the mole ratio of one. The ferrous chloride solution was freshly prepared by dissolving iron metal powder (Merck, Germany) in concentrated hydrochloric acid under CO_2 atmosphere.

Preparation of hydrazinated mixed nickel manganese zinc ferrous fumarate complexes

The synthesis of hydrazinated mixed manganese nickel zinc ferrous fumarates was carried out using fumarato hydrazinate precursor method [43–45]. The stoichiometric mixture of sodium fumarate and hydrazine hydrate was prepared by mixing aqueous sodium fumarate (3 M) and hydrazine hydrate (6 M) in 1:2 molar ratios and stirred continuously for 2 h under nitrogen atmosphere in a 3-neck flask. The mixed metal chlorides (1 M) solution containing zinc chloride, nickel chloride and manganese chloride was mixed with freshly prepared ferrous chloride solution (2 M) and the solution was added dropwise, to the sodium fumarate and hydrazine hydrate mixture under nitrogen atmosphere. The yellow-coloured precipitate of hydrazinated mixed nickel manganese zinc ferrous fumarate complex obtained was filtered, washed thoroughly with ethanol for complete removal of chloride impurities, dried with diethyl ether on suction and stored in vacuum desiccator. The reaction may be represented as follows:

$$\begin{aligned} &x\mathrm{MnCl}_{2(\mathrm{aq})} + (0.6 - x)\mathrm{NiCl}_{2(\mathrm{aq})} + 0.4\mathrm{ZnCl}_{2(\mathrm{aq})} \\ &+ 2\mathrm{FeCl}_{2(\mathrm{aq})} + 3\mathrm{C_4H_2O_4Na_{2(aq)}} + 6\mathrm{N_2H_4 \cdot H_2O_{(aq)}} \\ &\rightarrow \mathrm{Mn_xNi_{0.6-x}Zn_{0.4}Fe_2(C_4H_2O_4)_3{\cdot}6N_2H_{4(s)}} + 6\mathrm{NaCl_{(aq)}} \\ &+ 6\mathrm{H_2O_{(l)}}\left(x = 0.2,\ 0.4 \text{ and } 0.1,\ \mathrm{M} = \mathrm{Ni^{2+}}, \mathrm{Mn^{2+}}, \mathrm{Zn^{2+}}\right) \end{aligned}$$

Characterization

The molecular compositions of hydrazinated mixed nickel manganese zinc ferrous fumarate complexes were fixed based on the chemical analyses results. The hydrazine content in the complexes was determined by titrimetric analysis using standard 0.025 M KIO_3 solution under Andrew's conditions [46]. The metal contents in the complexes were determined by chemical analyses after decomposing the known amount of precursors with concentrated nitric acid using standard procedures [46]. The iron and nickel content was determined gravimetrically as ferric oxide and nickel-dimethylglyoximato complex, respectively, while manganese and zinc were estimated together by complexometric titration using suitable masking agent [46]. The simultaneous thermogravimetry-differential scanning calorimetry (TG-DSC) measurements were performed using NETZSCH DSC-DTA-TG STA 409PC setup equipped with control and data acquisition system. The analyses were carried out in air (100 mL min^{-1}) at a heating rate of 10 °C min^{-1} using 15–20 mg sample in an alumina crucible with another alumina crucible as the reference material. The thermal analysis was carried out from room temperature to 800 °C. The isothermal mass loss studies of the complexes were carried out along with hydrazine analysis from room temperature to 125 °C by placing the accurately weighed complex (0.5 g) in silica crucible in the programmable electric oven with the heating rate of 2 °C min^{-1}. The total mass loss was determined by placing the accurately weighed quantity (1 g) of complex in silica crucible in muffle furnace maintained at 500 °C for 30 min. The infrared spectra of the complexes and thermal decomposition residues were recorded from 4,000–300 cm^{-1} in diffuse reflectance mode using FTIR Shimadzu IR prestige21 series spectrophotometer. The thermal decomposition residues were analysed for structure and phase purity using Philips X-ray diffractometer model PW 1710 with CuK_α radiations and Ni filter at room temperature. The TEM studies were carried out on Philips-CM20 electron microscope.

Results and discussion

The analytical data of the complexes (Table 1) obtained from chemical and thermal analyses were found to be in good agreement with the values calculated considering the molecular stoichiometric composition as $Mn_xNi_{0.6-x}Zn_{0.4}Fe_2(C_4H_2O_4)_3{\cdot}6N_2H_4$ ($x = 0.2$, 0.4 and 0.5) for hydrazinated mixed nickel manganese zinc ferrous fumarate complexes.

The infrared spectra (Fig. 1) of all the complexes are similar and display four bands in the region 3,307–3,163 cm^{-1} characteristic of N–H stretching frequency. The observed N–N stretching frequencies in the region 979–972 cm^{-1} for all the hydrazinated complexes clearly indicate the bidentate bridging coordination of hydrazine ligands to the central metal ion [47, 48]. The infrared frequencies characteristic of C=C stretching are observed in the region 1,646–1,630 cm^{-1} in all the complexes [15]. The dicarboxylate ions in the complexes coordinate with the metal ions as a bidentate ligand via both the carboxylate groups. In all the complexes the asymmetric stretching (ν_{as}) vibrations of the carboxylate ions are observed in the region 1,586–1,583 cm^{-1} and the symmetric stretching (ν_s) vibrations are seen in the region 1,382–1,374 cm^{-1} with the separation $\Delta\nu$ (ν_{as}–ν_s) of 201–212 cm^{-1}. This wide separation between ν_{as} (COO^-) and ν_s (COO^-) clearly indicates the monodentate coordination of the fumarate dianions [15, 32, 49]. Thus, the infrared spectroscopic result confirms the bidentate

Table 1 Chemical and thermal analysis results of hydrazinated mixed nickel manganese zinc ferrous fumarate complexes, $Mn_xNi_{0.6-x}Zn_{0.4}Fe_2(C_4H_2O_4)_3{\cdot}6N_2H_4$ ($x = 0.2$, 0.4 and 0.5)

Complex compo. (x)	Metal content/%								Hydrazine content/%		Total mass loss/%		Isothermal mass loss/hydrazine/%		
	Fe		Mn		Ni		Zn						RT–75 °C	75–100 °C	100–125 °C
	Obs.	Calc.	Obs.	Calc.	Obs.	Calc.	Obs.	Calc.	Obs.	Calc.	Obs.	Calc.			
0.2	15.78	15.80	1.54	1.56	3.31	3.32	3.68	3.70	27.21	27.21	67.08	66.56	2.12/27.24	54.34/–	–
0.4	15.80	15.82	3.09	3.11	1.62	1.66	3.66	3.71	27.49	27.23	66.67	66.64	1.47/27.50	56.46/–	–
0.5	15.81	15.83	3.83	3.89	0.824	0.832	3.69	3.71	27.29	27.25	66.72	66.67	2.03/27.20	2.35/25.4	56.75/–

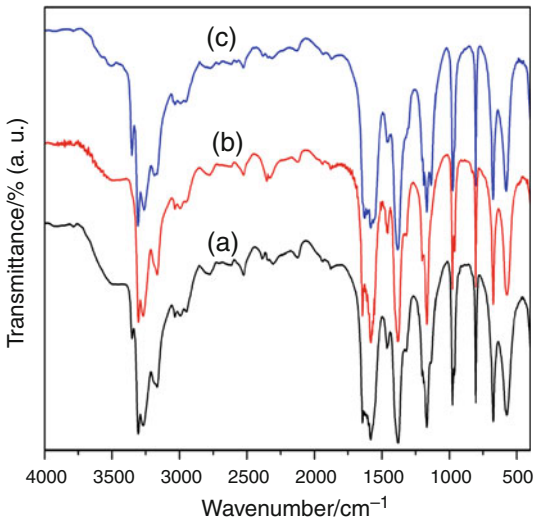

Fig. 1 FTIR spectra of $Mn_xNi_{0.6-x}Zn_{0.4}Fe_2(C_4H_2O_4)_3{\cdot}6N_2H_4$ complexes, **a** $x = 0.2$, **b** $x = 0.4$ and **c** $x = 0.5$

bridging behaviour of neutral hydrazine ligands and monodentate linkage of fumarate dianion and hence the polymeric nature of the hydrazinated mixed nickel manganese zinc ferrous fumarate complexes with octahedral geometry around the metal ions [32]. Based on the chemical analyses results (Table 1) and infrared spectroscopic data the molecular composition assigned to these complexes is given in Table 2.

Thermal studies

The thermal decomposition of all the hydrazinated mixed nickel manganese zinc ferrous fumarate complexes was found to be self-propagating autocatalytic. For this autocatalytic decomposition, the complex was spread uniformly over a ceramic tile and ignited with a burning splinter at one of the corners. It catches fire and burns without flame forming a red glow which spreads over the entire bulk, completing the total decomposition in ordinary atmosphere. The thermal decomposition residues were found to be stoichiometrically pure and nanocrystalline $Mn_xNi_{0.6-x}Zn_{0.4}Fe_2O_4$ ($x = 0.2$, 0.4 and 0.5) ferrites.

TG-DSC and isothermal mass loss studies

Figures 2, 3 and 4 represent the simultaneous thermal (TG-DSC) curves of the hydrazinated mixed nickel manganese zinc ferrous fumarate complexes from room temperature to 800 °C at a heating rate 10 °C min^{-1}. All the hydrazinated mixed nickel manganese zinc ferrous fumarate complexes exhibit similar decomposition behaviour. The first step is the dehydrazination followed by oxidative decarboxylation. The dehydrazination occurs in two steps in complexes with, $x = 0.2$ (Fig. 2) and $x = 0.4$ (Fig. 3), while the complex with $x = 0.5$ (Fig. 4) shows three steps dehydrazination. The decarboxylation occurs in one step in all the complexes resulting into nanocrystalline $Mn_xNi_{0.6-x}Zn_{0.4}Fe_2O_4$ ($x = 0.2$, 0.4 and 0.5) ferrites as thermal decomposition residue. The initial mass loss of 1.45–2.45 % in TG curve of all the complexes from room temperature to 75 °C is due to desorption of the adsorbed species including moisture. The major mass loss of 22.94 and 24.57 %, respectively, in the region 75–110 °C in the

Table 2 Proposed molecular formulae of hydrazinated mixed nickel manganese zinc ferrous fumarate complexes and their thermal decomposition residue

Proposed molecular formula	Molecular mass	Thermal decomposition residue	Molecular mass
$Mn_{0.2}Ni_{0.4}Zn_{0.4}Fe_2(C_4H_2O_4)_3{\cdot}6N_2H_4$	706.8	$Mn_{0.2}Ni_{0.4}Zn_{0.4}Fe_2O_4$	236.11
$Mn_{0.4}Ni_{0.2}Zn_{0.4}Fe_2(C_4H_2O_4)_3{\cdot}6N_2H_4$	706	$Mn_{0.4}Ni_{0.2}Zn_{0.4}Fe_2O_4$	235.56
$Mn_{0.5}Ni_{0.1}Zn_{0.4}Fe_2(C_4H_2O_4)_3{\cdot}6N_2H_4$	705.6	$Mn_{0.5}Ni_{0.1}Zn_{0.4}Fe_2O_4$	235.18

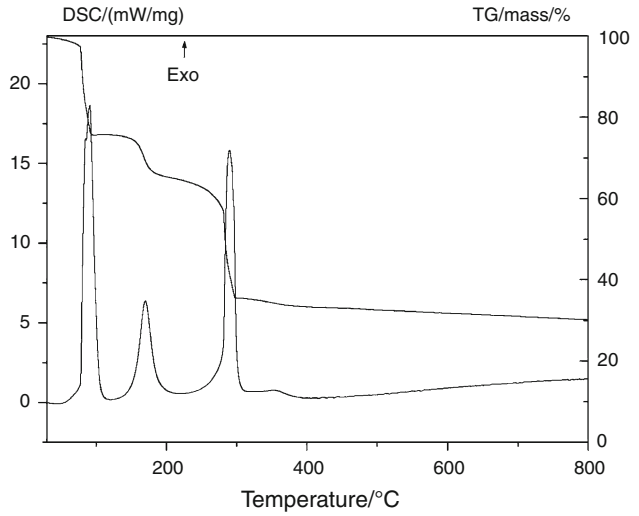

Fig. 2 TG-DSC curves of $Mn_{0.2}Ni_{0.4}Zn_{0.4}Fe_2(C_4H_2O_4)_3{\cdot}6N_2H_4$ complex

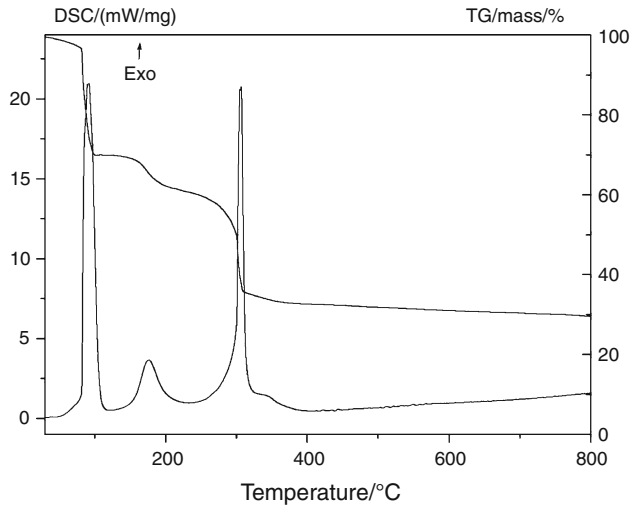

Fig. 3 TG-DSC curves of $Mn_{0.4}Ni_{0.2}Zn_{0.4}Fe_2(C_4H_2O_4)_3{\cdot}6N_2H_4$ complex

complexes with $x = 0.2$ and 0.4 corresponds to the loss of five hydrazine molecules. This dehydrazination is highly exothermic as indicated by strong exothermic peak at 91.9 °C (Fig. 2) and 91 °C (Fig. 3), respectively, in DSC curve. The complex with $x = 0.5$ shows mass loss of 1.9 % in region 75–110 °C with weak exothermic peak at 85.9 °C in DSC curve, which is an indication of beginning of the dehydrazination. The major mass loss of 22.98 % observed in complex with $x = 0.5$ from 110 to 150 °C is in agreement with the theoretically calculated value corresponding to the loss of five hydrazine molecules. The DSC curve shows strong exothermic peak at 139 °C corresponding to this hydrazine loss. The next region in the TG curve of all the complexes with mass loss of 4.53–7.56 % (Table 3) from 150 to 230 °C is due to the loss of a hydrazine

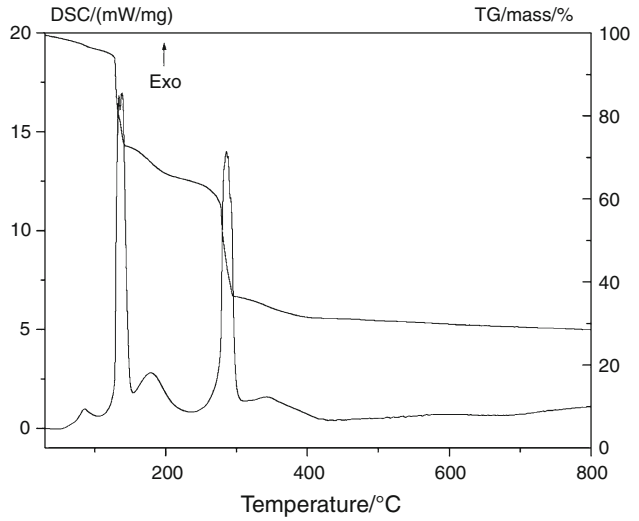

Fig. 4 TG-DSC curves of $Mn_{0.5}Ni_{0.1}Zn_{0.4}Fe_2(C_4H_2O_4)_3{\cdot}6N_2H_4$ complex

molecule and simultaneous beginning of decarboxylation. The major mass loss region of 28.17–35.38 % in TG curve from 230 to 330 °C results from the oxidative decarboxylation of dehydrazinated complexes. This decarboxylation is marked by strong exothermic peak at 289, 307 and 286 °C in the DSC curve of complexes with $x = 0.2$, $x = 0.5$ and $x = 0.4$, respectively. The mass loss of 4.5–6.38 % in TG curve of complexes from 330 to 440 °C is due to the oxidation of residual carbon formed during the decarboxylation. The DSC curve shows broad exothermic hump in this temperature region.

The thermal behaviour of these complexes was also investigated by isothermal mass loss studies at temperatures derived from TG curve wherein the thermal changes in the complexes were observed. The isothermal mass loss studies in air of complexes with $x = 0.2$ and 0.4 shows mass loss of 2.2 and 1.47 % (Table 1), respectively, from room temperature to 75 °C, but the hydrazine analysis shows increase in its value which indicates that the mass loss is not due to hydrazine loss but due to the adsorbed species including moisture. In these complexes the dehydrazination begins above 75 °C followed by the self-propagating autocatalytic decomposition behaviour in the temperature range 75–100 °C. The complex with $x = 0.5$ shows continuous mass loss from room temperature to 100 °C which corresponds to the loss of hydrazine as observed from analysis of hydrazine which shows continuous decrease in its value up to 100 °C. For this complex the self-propagating autocatalytic decomposition behaviour is observed in the temperature region 100–125 °C.

The total mass loss (Table 1) obtained from TG curve and that obtained independently from the pyrolysis in air matches well with the calculated values considering the molecular composition of the complexes as

Table 3 TG-DSC data of hydrazinated mixed nickel manganese zinc ferrous fumarate complexes, $Mn_xNi_{0.6-x}Zn_{0.4}Fe_2(C_4H_2O_4)_3{\cdot}6N_2H_4$ ($x = 0.2$, 0.4 and 0.5)

Complex compo. (x)	Temperature range/°C, mass loss (TG)/%, DSC/°C						
	RT–75	75–110	110–150	150–230	230–330	330–440	RT–440
0.2	1.45	22.94/91.9 (exo)	–	4.53/170 (exo)	35.38/289 (exo)	4.50/345-390 (broad exo hump)	68.80
0.4	2.45	24.57/91 (exo)	–	7.56/177 (exo)	28.17/307(exo)	3.42/340-37 (broad exo hump)	68.66
0.5	2.40	1.9/85.9 (exo)	22.98/139 (exo)	5.84/179 (exo)	28.32/286 (exo)	6.38/335-360 (broad exo hump)	66.18
Remark		2-step dehydrazination			1-step decarboxylation		

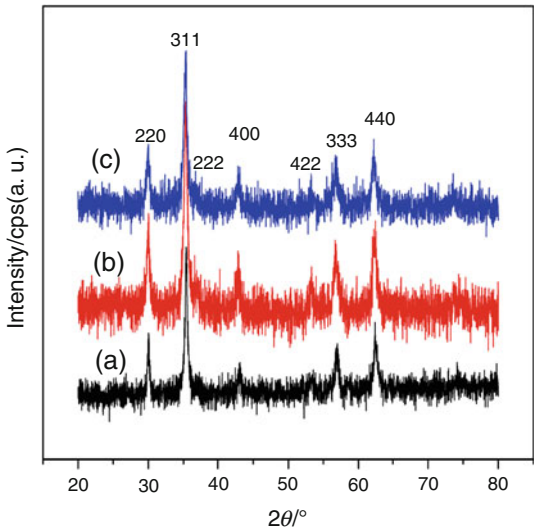

Fig. 5 X-ray diffraction patterns of $Mn_xNi_{0.6-x}Zn_{0.4}Fe_2O_4$ ferrites, **a** $x = 0.2$, **b** $x = 0.4$ and **c** $x = 0.5$

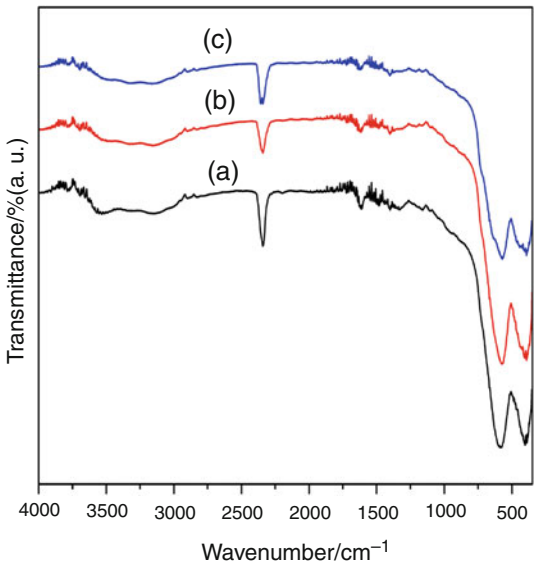

Fig. 6 FTIR spectra of $Mn_xNi_{0.6-x}Zn_{0.4}Fe_2O_4$ ferrites, **a** $x = 0.2$, **b** $x = 0.4$ and **c** $x = 0.5$

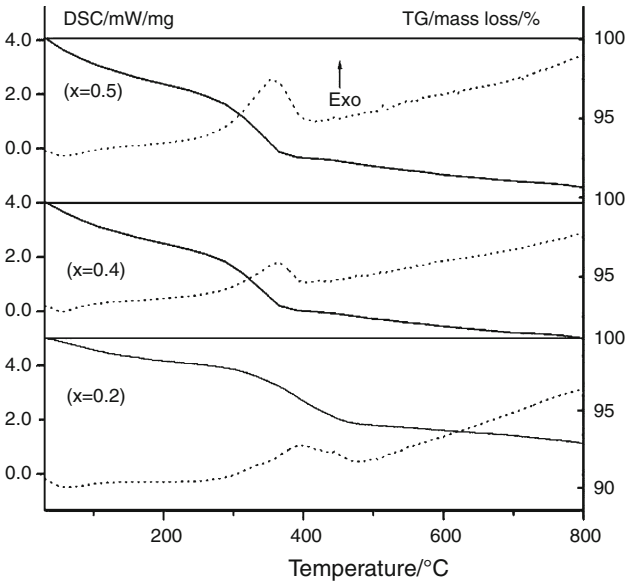

Fig. 7 TG-DSC curves of $Mn_xNi_{0.6-x}Zn_{0.4}Fe_2O_4$ ferrites, **a** $x = 0.2$, **b** $x = 0.4$ and **c** $x = 0.5$

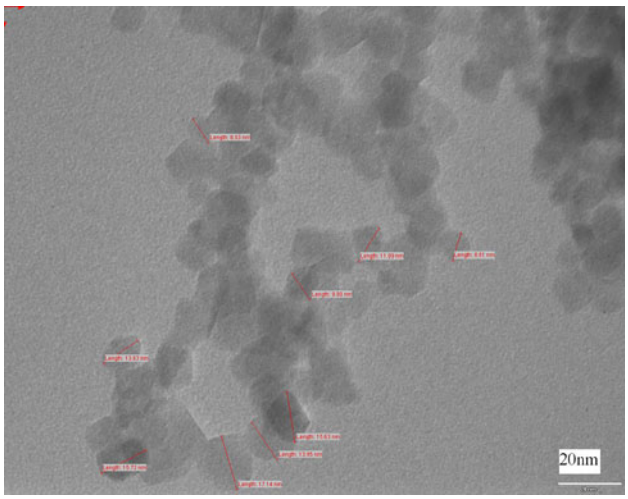

Fig. 8 TEM of $Mn_{0.5}Ni_{0.1}Zn_{0.4}Fe_2O_4$ ferrite

$Mn_xNi_{0.6-x}Zn_{0.4}Fe_2(C_4H_2O_4)_3{\cdot}6N_2H_4$ ($x = 0.2$, 0.4 and 0.5) and the thermal decomposition residue as $Mn_xNi_{0.6-x}Zn_{0.4}Fe_2O_4$ ($x = 0.2$, 0.4 and 0.5).

The thermal decomposition residues obtained after the self-propagating autocatalytic decomposition of the complexes were analysed for their phase purity and ultrafine nature. The X-ray diffraction patterns of all the thermal decomposition residues (Fig. 5) were identical and display all the peaks characteristics of cubic spinel ferrite without any noticeable impurity peak [50]. The broadening of peaks indicates their nanocrystalline nature. The average crystallite size calculated using Scherrer formula lies in the range 14–21 nm. The infrared spectra of the thermal decomposition residues (Fig. 6) show two bands in the region 586–572 and 410–380 cm^{-1} which are characteristic of metal–oxygen stretching vibrational frequencies in tetrahedral (A) and octahedral (B) sites in cubic spinel lattice [51, 52], thus supporting the formation of $Mn_xNi_{0.6-x}Zn_{0.4}Fe_2O_4$ ($x = 0.2$, 0.4 and 0.5) ferrites. The monophasic nature of thermal decomposition residues were also established from TG-DSC measurements. The TG curves (Fig. 7) show two mass loss regions, the mass loss region up to 100 °C is due to the loss of physisorbed moisture and the region from 300 to 440 °C corresponds to the oxidation of residual carbon formed during decarboxylation. A weak endothermic peak corresponding to desorption and the broad exothermic humps which correspond to oxidation of residual carbon was observed in the DSC curves of the thermal decomposition residues. Besides these two mass loss regions the TG-DSC curves are very stable up to 800 °C, which confirms the absence of any metastable phase like γ-Fe_2O_3 which could not be otherwise detected in the X-ray diffraction pattern. The nanosize nature of $Mn_xNi_{0.6-x}Zn_{0.4}Fe_2O_4$ ($x = 0.2$, 0.4 and 0.5) ferrites suggested from the broadening of X-ray diffraction peaks was confirmed by carrying out TEM measurements. The representative TEM image (Fig. 8) shows the uniform distribution of nanosize particles with particle size in the range 8–23 nm which is in tune with that obtained from X-ray diffraction studies.

Conclusions

The hydrazinated mixed nickel manganese zinc ferrous fumarate complexes were synthesized from sodium fumarate, metal chloride and hydrazine hydrate at room temperature. The chemical analyses, total mass loss and infrared spectroscopic studies of the complexes confirm the formation with stoichiometric composition viz. $Mn_xNi_{0.6-x}Zn_{0.4}Fe_2(C_4H_2O_4)_3{\cdot}6N_2H_4$ ($x = 0.2$, 0.4 and 0.5). The TG-DSC studies of the complexes show two-step dehydrazination followed by one-step oxidative decarboxylation. The complexes display self-propagating autocatalytic decomposition behaviour once ignited, to give nanocrystalline $Mn_xNi_{0.6-x}Zn_{0.4}Fe_2O_4$ ($x = 0.2$, 0.4 and 0.5) ferrites as the thermal decomposition residue. The X-ray diffraction patterns of thermal decomposition residue indicates the formation of the monophasic $Mn_xNi_{0.6-x}Zn_{0.4}Fe_2O_4$ ($x = 0.2$, 0.4 and 0.5) ferrites. The broadening of X-ray diffraction peaks indicates nanosize nature of $Mn_xNi_{0.6-x}Zn_{0.4}Fe_2O_4$ ($x = 0.2$, 0.4 and 0.5) ferrite particles which is confirmed by TEM analysis with the particle size in the range 8–23 nm.

Acknowledgments Authors are grateful for the financial support from DST, New Delhi through the Nano Mission project, No. SR/NM/NS-86/2009 and also under FIST. The authors are also thankful to UGC, New Delhi for the financial support under SAP and minor research project. The authors would like to acknowledge SAIF-IIT Bombay and Mr. Girish Prabhu, N.I.O., Goa for recording TEM micrograph and XRD of the samples, respectively.

References

1. Randhawa BS, Sweety K. Calcium ferrite formation from the thermolysis of calcium tris(maleato)ferrate(III). Bull Mater Sci. 2000;23(4):305–7.
2. Randhawa BS, Kaur M, Gandotra K. Synthesis of nanosized ferrites from the thermolysis of strontium and barium hexa(formato)ferrates(III). J Radioanal Nucl Chem. 2006;269(1):69–74.
3. Randhawa BS, Gandotra K. Preparation of ferrites from the thermal decomposition of magnesium and calcium tris(succinato)ferrates(III)precursors. J Therm Anal Calorim. 2007;90(3):887–91.
4. Randhawa BS. Thermal analysis of manganese hexa(formato)ferrate(III)hexahydrate. J Radioanal Nucl Chem. 1997;220(2):237–9.
5. Logvinenko V, Polunina O, Mikhailov Yu, Mikhailov K, Bokhonov B. Study of thermal decomposition of silver acetate. J Therm Anal Calorim. 2007;90(3):813–6.
6. Ubaldini A, Artini C, Costa GA, Carnasciali MM, Masini R. Thermal decomposition of mixed Ce and Gd oxalates and thermal properties of mixed Ce and Gd oxides. J Therm Anal Calorim. 2006;84(1):207–11.
7. Deb N. Thermal decomposition of manganese(II)bis(oxalato)nickelate(II) tetrahydrate. J Therm Anal Calorim. 2005;81:61–5.
8. Deb N. Thermal investigations of $M[La(C_2O_4)_3]{\cdot}xH_2O$ (M = Cr(III) and Co(III)). J Therm Anal Calorim. 2002;67:699–712.
9. Randhawa BS, Kaur S, Bassi PS. Thermal decomposition of strontium and barium malonates. J Therm Anal Calorim. 1999;55:789–96.
10. Amghouz Z, Roces L, García-Granda S, García JR, Souhail B, Mafra L, Shi F, Rocha J. Yttrium-succinates coordination polymers: hydrothermal synthesis, crystal structure and thermal decomposition. J Solid State Chem. 2009;182:3365–73.
11. Carp O, Patron L, Pascu G, Mindru L, Stanica N. Thermal investigation of nickel–zinc ferrites formation from malate coordination compounds. J Therm Anal Calorim. 2006;84(2):391–4.
12. Randhawa BS, Kaur M. The thermolysis of zinc bis(citrato)ferrate(III) dodecahydrate. J Radioanal Nucl Chem. 2003;256(3):509–11.
13. Deb N. Thermal decomposition behavior of lanthanum (III) tris-tartrato lanthanate(III) decahydrate. J Therm Anal Calorim. 2004;78:227–37.

14. Randhawa BS, Sweety KJ, Kaur M, Greneche JM. Synthesis of ferrites: thermal analysis of some transition metal tris(maleato)ferrates(III). J Therm Anal Calorim. 2004;75:101–11.
15. Porollo NP, Aliev ZG, Dzhardimalieva GI, Ivelva IN, Uflyand IE, Pomogailo AD, Ovenesyan NS. Synthesis and structure of salts of unsaturated dicarboxylic acids. Russ Chem Bull. 1997;46(2): 362–70.
16. Randhawa BS, Kaur M. A comparative study on the thermal decomposition of some transition metal maleates and fumarates. J Therm Anal Calorim. 2007;89(1):251–5.
17. Zhu WH, Wang ZM, Gao SA. 3D porous lanthanide-fumarate framework with water hexamer occupied cavities, exhibiting a reversible dehydration and rehydration procedure. Dalton Trans. 2006;(6):765–8.
18. Manna SC, Zangrando E, Ribas J, Chaudhuri NR. Carboxylato-bridged 3D polymeric networks of Gd(III): synthesis, crystal structure, magnetic property and thermal behaviour. Polyhedron. 2006;25:1779–86.
19. Allan JR, Bonner JG, Bowley HJ, Gerrard DL, Hoey S. Thermal studies on fumaric acid and crotonic acid compounds of cobalt(II) and nickel(II). Thermochim Acta. 1989;141:227–33.
20. Ionashiro EY, Caires FJ, Siqueira AB, Lima LS, Carvalho CT. Thermal behaviour of fumaric acid, sodium fumarate and its compounds with light trivalent lanthanides in air atmosphere. J Therm Anal Calorim. 2012;108:1183–8.
21. Carr NJ, Galwey AK. The thermal decomposition reactions of copper(II) maleate and of copper(II) fumarate. J Chem Soc Faraday Trans. 1998;84:1357–73.
22. Ravindranathan P, Patil KC. Thermal reactivity of metal formate hydrazinates. Thermochim Acta. 1983;71:53–7.
23. Mahesh GV, Patil KC. Thermal reactivity of metal acetate hydrazinates. Thermochim Acta. 1986;99(1):153–8.
24. Sivasankar BN, Govindrajan S. Acetate and malonate complexes of cobalt(II), nickel(II) and zinc(II) with hydrazinium cation: preparation, spectral and thermal studies. J Therm Anal. 1997;48(6):1401–13.
25. Gajapathy D, Patil KC, Pai Vernekar VR. Low temperature ferrite formation using metal oxalate hydrazinate precursor. Mater Res Bull. 1982;17(1):29–32.
26. Gajapathy D, Patil KC. Mixed metal oxalate hydrazinates as compound precursors to spinel ferrites. Mater Chem Phys. 1983;9:423–38.
27. Gajapathy D, Patil KC, Kishore K. Thermal reactivity of metal oxalate hydrazinates. Thermochim Acta. 1982;52:113–20.
28. Sivasankar BN, Govindarajan S. Hydrazine mixed metal malonates—new precursors for metal cobaltites. Mater Res Bull. 1996;31(1):47–54.
29. Sivasankar BN, Govindarajan S. Studies on bis(hydrazine) metal malonates and succinates. Synth React Inorg Met-Org Chem. 1994;24(9):1573–82.
30. Sivasankar BN. Cobalt(II), nickel(II) and zinc(II) dicarboxylate complexes with hydrazine as bridged ligand characterization and thermal degradation. J Therm Anal Calorim. 2006;86(2):385–92.
31. Verenkar VMS, Rane KS. Synthesis, characterisation and thermal analysis of ferrous malato-hydrazinate 'In: Ravindran PV, Sudersanan M, Misra NL, Venugopal V editors. Proceedings of the 12th national symposium on thermal analysis, Thermans 2000. Gorakhpur, India: Indian Thermal Analysis Society; 2000. pp. 194–95.
32. Govindrajan S, Banu SUN, Sarayanan N, Sivasankar BN. Bis-hydrazine metal maleates and fumarates: preparation, spectral and thermal studies. Proc Indian Acad Sci (Chem Sci.). 1995;107(5):559–65.
33. Sawant SY, Verenkar VMS, Mojumdar SC. Preparation, thermal, XRD, chemical and FTIR spectral analysis of $NiMn_2O_4$ nanoparticles and respective precursor. J Therm Anal Calorim. 2007;90(3):669–72.
34. More A, Verenkar VMS, Mojumdar SC. Nickel ferrite nanoparticles synthesis from novel fumarato-hydrazinate precursor. J Therm Anal Calorim. 2008;94(1):63–7.
35. Gawas UB, Verenkar VMS, Mojumdar SC. Synthesis and characterization of $Ni_{0.6}Zn_{0.4}Fe_2O_4$ nano-particles obtained by auto catalytic thermal decomposition of carboxylato–hydrazinate complex. J Therm Anal Calorim. 2011;104(3):879–83.
36. Gawas UB, Mojumdar SC, Verenkar VMS. Synthesis, characterization, infrared studies, and thermal analysis of $Mn_{0.6}Zn_{0.4}Fe_2(C_4H_2O_4)_3{\cdot}6N_2H_4$ and its decomposition product $Mn_{0.6}Zn_{0.4}Fe_2O_4$. J Therm Anal Calorim. 2010;100(3):867–71.
37. Gonsalves LR, Verenkar VMS, Mojumdar SC. Preparation and characterization of $Co_{0.5}Zn_{0.5}Fe_2(C_4H_2O_4)_3{\cdot}6N_2H_4$. A precursor to prepare $Co_{0.5}Zn_{0.5}Fe_2O_4$ nanoparticles. J Therm Anal Calorim. 2009;96(1):53–7.
38. Gonsalves LR, Mojumdar SC, Verenkar VMS. Synthesis and characterization of $Co_{0.8}Zn_{0.2}Fe_2O_4$ nanoparticles. J Therm Anal Calorim. 2011;104(3):869–73.
39. Gonsalves LR, Mojumdar SC, Verenkar VMS. Synthesis and characterization of ultrafine spinel ferrites obtained by precursor combustion technique. J Therm Anal Calorim. 2012;108:859–63.
40. Gonsalves LR, Verenkar VMS. Synthesis and thermal studies of the cobalt zinc ferrous fumarato-hydrazinate: a precursor to obtained nanosize ferrites. J Therm Anal Calorim. 2012;108:871–5.
41. Gonsalves LR, Mojumdar SC, Verenkar VMS. Synthesis of cobalt nickel ferrite nanoparticles via autocatalytic decomposition of the precursor. J Therm Anal Calorim. 2010;100(3):789–92.
42. Gonsalves LR, Verenkar VMS. Synthesis and characterization of nanosize nickel doped cobalt ferrite obtained by precursor combustion technique. J Therm Anal Calorim. 2012;108:877–80.
43. Gawas UB, Mojumdar SC, Verenkar VMS. $Ni_{0.5}Mn_{0.1}Zn_{0.4}Fe_2(C_4H_2O_4)_3{\cdot}6N_2H_4$ precursor $Ni_{0.5}Mn_{0.1}Zn_{0.4}Fe_2O_4$ nanoparticles preparation, IR spectral, XRD, SEM-EDS and thermal analysis. J Therm Anal Calorim. 2009;96(1):49–52.
44. Gawas UB, Verenkar VMS, Mojumdar SC. Nano-crystalline $Mn_{0.3}Ni_{0.3}Zn_{0.4}Fe_2O_4$ obtained by novel fumarato-hydrazinate precursor method: synthesis, characterization and studies of magnetic and electrical properties. J Therm Anal Calorim. 2012;108:865–70.
45. Gawas UB, Verenkar VMS. Synthesis, thermo-analytical and IR spectral studies of hydrazinated mixed metal carboxylates: a single source precursor to nanosize mixed metal oxides. Thermochim Acta. 2013;556:41–56.
46. Vogel's, Text book of quantitative inorganic analysis (Revised by Jeffery GH, Bassett V, Mendham J and Denney RC), 5th edn. Longman, UK; 1989. p. 334-335, 402,457,462.
47. Braibanti A, Dallavalle F, Pellinghelli MA, Leporati E. The nitrogen–nitrogen stretching band in hydrazine derivatives and complexes. Inorg Chem. 1968;7:1430–3.
48. Tsuchiya R, Yonemura M, Uehera A, Kyuno E. Derivatographic studies on transition metal complexes. XIII. Thermal decomposition of $[Ni(N_2H_4)_6]X_2$ complexes. Bull Chem Soc Jpn. 1974; 47(3):660–4.
49. Nakamoto K. Infrared and Raman spectra of inorganic and coordination compounds part B, 6th ed. New York: Wiley; 1978. p. 13.
50. Mane DR, Birajdar DD, Shirsat SE, Telugu RA, Kadam RH. Structural and magnetic characterizations of Mn–Ni–Zn ferrite nanoparticles. Phys Status Solidi A. 2010;207(10):2355–63.
51. Waldron RD. Infrared spectra of ferrites. Phys Rev. 1955;99: 1727–35.
52. Srinivasan TT, Srivastava CM, Venkataramani N, Patni MJ. Infrared absorption in spinel ferrites. Bull Mater Sci. 1984;6(6):1063–7.